Journal of
Manufacturing and Materials Processing

MDPI

Article

Process Developments in Electron-Beam Powder Bed Fusion Enabled by Near-Infrared Radiation

William Sjöström [1,*], Lars-Erik Rännar [1], Carlos Botero [1] and Laia Ortiz Membrado [2]

[1] SportsTech Research Center, Mid Sweden University, 831 40 Östersund, Sweden; lars-erik.rannar@miun.se (L.-E.R.); carlos.botero@miun.se (C.B.)
[2] Barcelona Research Center in Multiscale Science and Engineering, Universitat Politècnica de Catalunya, Campus Diagonal Besòs—EEBE, 08019 Barcelona, Spain; laia.ortiz@upc.edu
* Correspondence: william.sjostrom@miun.se

Abstract: The use of an electron beam (EB) as a heating source in EB-based powder bed fusion (PBF-EB) has several limitations, such as reduced powder recyclability, short machine service intervals, difficulties with heating large areas and the limited processability of charge-sensitive powders. Near-infrared (NIR) heating was recently introduced as a feasible replacement and/or complement to EB heating in PBF-EB. This work further investigates the feasibility of using NIR to eliminate the need for a build platform as well as to enable easier repairing of parts in PBF-EB. NIR-assisted Ti-6Al-4V builds were successfully carried out by starting from a loose powder bed without using a build platform. The results do not only confirm that it is possible to eliminate the build platform by the aid of NIR, but also that it can be beneficial for the process cleanliness and improve the surface quality of built parts. Furthermore, a 430 stainless-steel (SS) component could be repaired by positioning it in a loose 316L SS powder bed using a fully NIR-heated PBF-EB process.

Keywords: electron beam; powder bed fusion; near-infrared heating; process manipulation; additive manufacturing; 316L; stainless steel; Ti-6Al-4V

Citation: Sjöström, W.; Rännar, L.-E.; Botero, C.; Membrado, L.O. Process Developments in Electron-Beam Powder Bed Fusion Enabled by Near-Infrared Radiation. *J. Manuf. Mater. Process.* **2024**, *8*, 211. https://doi.org/10.3390/jmmp8050211

Academic Editor: Steven Y. Liang

Received: 6 August 2024
Revised: 20 September 2024
Accepted: 23 September 2024
Published: 26 September 2024

1. Introduction

Electron-beam powder bed fusion (PBF-EB) is an additive manufacturing (AM) technology, in which metal components are produced layer by layer from a powder feedstock. The fast movement of the electron beam (EB) inside a controlled vacuum atmosphere renders very good control over cleanliness and as-built material properties [1,2]. The cost of the process has so far limited the use to mainly high-performance parts and crack-sensitive alloys [3–9], but recently even ceramic materials have been processed [10,11]. As the process is performed at elevated temperatures inside a vacuum [12], it is known for producing dense parts with low residual stresses due to the minimal thermal gradients during solidification [13–15]. One of the benefits of this technology is that the powder can be reused in later processes, thereby minimizing the process waste [16,17].

The negative charge build-up, arising from the incident electrons upon impact with the powder, must be limited or extracted from the build area to avoid disruptions to the powder bed, known as "smoke" [17–22]. To allow fast heating rates, PBF-EB processes rely on a high-mass build platform which minimizes issues with smoke during the initial build stage. The build platform allows the full beam power to be applied during the initial heating up to a process temperature between 40% and 80% of the melting point of the processed alloy [23,24]. In the majority of industrial applications, 10 mm thick stainless-steel build platforms are used, although the shape and material can be governed by the specifics of the process and the targeted build material [25]. It is a foreseen issue that the build platform material may contaminate the manufactured alloy if the chemical compositions are not identical, which they often are not. Most PBF-EB processes are conducted on stainless-steel build platforms regardless of the feedstock alloy. Although

there are countless investigations on, for instance, how the mechanical properties are affected by varying the location of the parts in the build chamber [26–29], no publication could be found on how contamination from the build platform affects the built parts. Further, Derimow et al. noticed an increased O_2 pickup in the powder cake close to the build platform [30], and it is not unlikely that the plate could cause outgassing, which can further activate smoke events in some cases [31].

LASER-based PBF (PBF-LB) also utilizes build platforms, but in such cases, there are no issues with powder charging. The motivation for using build platforms in PBF-LB is commonly to increase the thermal transfer, reduce warpage by providing mechanical support and decrease the cracking susceptibility of the built parts [32–34]. As PBF-EB is a hot process and the powder cake provides some support for the parts, these functions of a build plate are not as critical. To the best knowledge of the authors, there are no publications available which describe PBF AM having been performed without a build platform; thus, it is not entirely clear what the potential drawbacks of removing the build platform would be.

The use of build platforms also complicates the possibility for cold restarts or for repairing parts in PBF-EB. Repairing parts by AM has been researched [35–43], and theoretically PBF-EB should be good at creating a solid repair even on the microstructural level. However, pre-heating a large volume of loose, cold powder with an EB is difficult compared to PBF-LB, where the fixtures for the parts to be repaired can be placed in the loose powder [36,39]. Parts to be repaired by PBF-EB commonly have to be in the form of a build platform or press-fitted into a modified build platform before the repairing process starts [25,40,44–46]. Replacing and leveling the build platform before each build also adds to the process preparation time and manufacturing costs. Further adding to the cost, alloys similar to the build platform material will fully fuse to it, meaning that processes such as mechanical cutting and electric discharge machining (EDM) are needed post-manufacturing. This increases the post-processing cost and must be considered when designing the build layout so that the parts are not damaged upon removal.

Recently, near-infrared (NIR) heating was shown to be a promising complement to the PBF-EB process by allowing quick, charge-free heating of the powder in each layer [47]. The introduction of NIR technology also reduced the EB build cost, improved powder recyclability by reducing scrap and increased the service intervals of electron gun parts [47]. Due to the promising results, NIR may also allow additional benefits in PBF-EB processes, such as bulk heating of the powder around a component to be repaired or quick heating of a loose powder bed, which could eliminate the need for a build platform. This work evaluates how NIR can assist PBF-EB to solve the issues discussed above, for instance, by making the process or as-built material properties better, and to simplify the repairing of parts.

The experiments involved processing Ti-6Al-4V and 316L powders, as they present different challenges and have important roles in PBF-EB. Ti-6Al-4V is one of the "original" materials for PBF-EB and has been highly researched [48,49]. This material is currently used in industry, where upscaling and optimized processes are of the essence [50]. The microstructure of PBF-EB-produced Ti-6Al-4V commonly consists of columnar beta grains separated by alpha-grain boundaries. Due to the transformation upon cooling from the β phase (BCC) to α (HCP) and α′ phases (sheared HCP due to rapid cooling, sometimes referred to as the martensitic phase), the beta grains contain an intergranular α "basket-weave" structure known as the Widmanstätten structure [51–53], where smaller laths have been reported to yield a higher strength [51]. The amount of β phase will depend on the thermal conditions, where areas with high heat retention (such as close to a build plate) will tend to result in more β phase [53]. Some α′ phase can be retained [53], but due to the high temperatures of PBF-EB the amount is generally quite small and located close to the top section of the build where less annealing is possible [53,54]. Although not as well researched as Ti-6Al-4V, the austenitic (FCC) 316L stainless-steel alloy has been produced by PBF-EB for almost 10 years [14,55]. PBF-EB-produced 316L commonly forms columnar grains with Cr- or Mo-enriched σ-phase (primitive tetragonal) precipitation in the grain boundaries [56]. The

σ phase will act to both embrittle the material and reduce the corrosion properties, as the surrounding area is depleted of Cr. Inside the austenitic grains, there is a cellular substructure, usually aligned with the build direction, outlined by Cr- and Mo-segregated boundaries [56,57].

2. Materials and Methods

2.1. Powders

Two feedstock powders were used in the experiments: alloy Ti-6Al-4V and 316L. The plasma-atomized Ti-6Al-4V of the 45–105 µm fraction was delivered by Arcam (Arcam AB, Mölndal, Sweden, now a part of GE Colibrium Additive, Pittsburgh, PA, USA). The gas-atomized 316L powder of fraction 53–150 µm was delivered by Carpenter (Carpenter powder products AB, Torshälla, Sweden). The flowability of both powders was evaluated according to ASTM B213 and yielded 20 s/50 g for 316L and 24 s/50 g for Ti-6Al-4V. The apparent density according to ASTM B213 was 4.89 g/cm^3 for 316L and 2.49 g/cm^3 for Ti-6Al-4V.

2.2. Sample Manufacturing

Samples were produced by conventional PBF-EB as well as by variations of NIR-assisted PBF-EB in the Arcam S12 system modified according to a previous publication [47] and equipped with a 6 kW NIR heater [47]. The different variants of NIR assistance for each experiment are described in Sections 2.2.1 and 2.2.2.

2.2.1. Build without a Build Platform with the Aid of NIR Heating

To test NIR-assisted PBF-EB without a build platform, the loose Ti-6Al-4V powder bed was heated by 6 kW NIR for 13 min, which created a hard and hot (red-glowing) quasi-platform for the build. The Arcam S12 system is conventionally only equipped with a K-type thermocouple (TC) placed under the build platform for monitoring the process temperature. Corresponding TC control in this case was problematic due to the limited thermal conduction of powder in a vacuum. Thereby, the color and glow intensity of the top layer relative to standard PBF-EB builds were used as indicators for the temperature. Further, 6 kW NIR heating applied for 13 min on a 150 mm × 150 mm × 10 mm build platform in the PBF-EB chamber corresponded to a TC reading of ~800 °C. This is slightly higher than the standard 730 °C processing temperature, but a higher temperature lowers the smoke sensitivity, which was the main concern when removing the build platform. It was assumed that the plate-free melting would require a higher starting temperature, as the thermal ballast commonly provided from the mass of the build platform was missing. After NIR heating, the standard PBF-EB process as provided by Arcam was used both for pre-heating and melting each layer on top of the quasi-platform. Samples were produced from the Ti-6Al-4V precursor powder. PBF-EB reference builds with EB heating and melting were conducted with the same build files on top of a 150 mm × 150 mm × 10 mm build platform in 304 stainless steel. Figure 1a shows the setup used for the reference builds, and Figure 1b shows the experimental setup used for NIR sintering a quasi-platform.

The build file was the same as presented in an earlier publication [47] and contained the following: four 15 mm × 15 mm × 15 mm cubes, four ⌀6 × 15 mm cylinders, one 55 mm × 2 mm × 15 mm block, one 25 mm × 25 mm × 14 mm triply periodic minimal surface (TPMS) lattice and one 25 mm × 55 mm × 2 mm block.

2.2.2. Repairing by NIR-Assisted PBF-EB

Repairing a part by PBF-EB can be problematic, as it involves heating a large volume of cold powder. To evaluate the feasibility of repairing parts by NIR-assisted PBF-EB, a special build was proposed, with the component "in need of reparation" having a non-planar upper surface. The component was a 125 mm long commercial teaspoon made from 430 stainless steel. The teaspoon was loaded at room temperature into the Arcam S12/A2 build chamber and placed in a loose 316L powder bed, as shown in Figure 1c, so that only a

small area was level with the powder-bed top surface. By centering the beam on the exposed area of the teaspoon, it was possible to align a build file to be built in the desired location. In this case, there was no need to further align the position of the object and the build file, but in other cases more points could be needed to align the build file axis with the object. The build file in this case contained a 10 mm high logotype for the research center. The experiment aimed at adding a solid 316L structure over the convex surface (oval 35 mm × 28 mm) of the teaspoon. NIR (6 kW) was applied both for initial heating and in each layer during the build; EB was used only for melting. The initial NIR heating was performed until the spoon was observed to be glowing red hot (4 min).

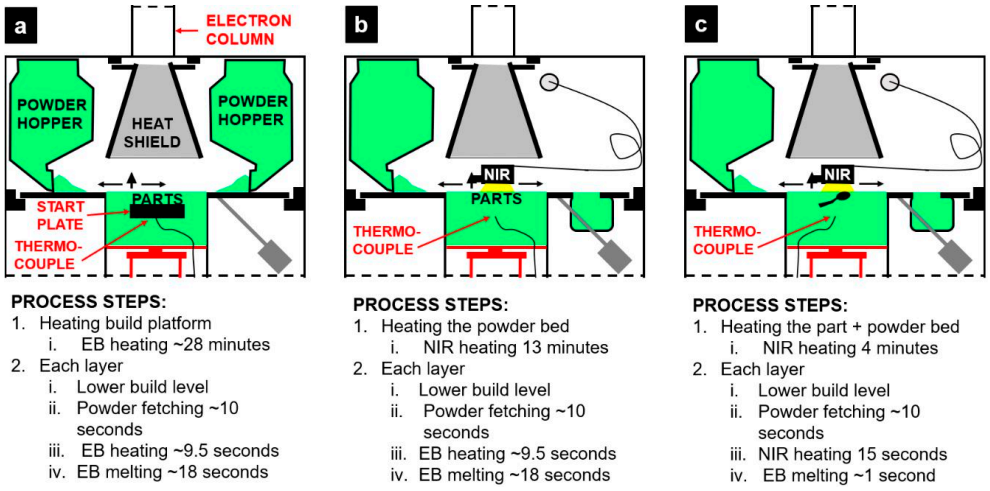

Figure 1. Illustrations of the standard PBF-EB setup that was used for manufacturing reference samples (**a**), the experimental setup used for melting parts without a build platform (**b**) and the experimental setup used for repairing parts (**c**).

2.3. Sample Characterization

Samples were characterized in terms of morphology and microstructure by scanning electron imaging (SEM; Tescan Maia 3, Brno, Czech Republic) energy-dispersive X-ray imaging (EDX; Oxford Instruments, Oxfordshire, UK) and in terms of hardness by micro-Vickers indentation (emcoTEST, DuraScan, Kuchl, Austria) according to SS-EN ISO 6507-1:2023 [58] for bulk sample hardness.

The micromechanical properties of selected areas on the Ti-6Al-4V samples were determined by nanoindentation (KLA, iMicro, Irvine, CA, USA) in load control mode. A diamond Berkovich tip was calibrated using a standard fused silica sample. The Nano-Blitz® 3D technique was used for mapping the elastic modulus (E) and hardness (H). A map of 200 µm × 200 µm was performed, with 200 × 200 nanoindentations with 1 µm spacings at a maximum load of 2 mN. The indentation depth was in the range of 80 nm to 110 nm depending on the location.

3. Results and Discussion

3.1. Build without a Build Platform with the Aid of NIR Heating

The NIR quasi-platform functioned as a starting platform, although there were some issues with warping of the first melted layers. This was to be expected, as sintered powder lacks the mechanical properties of a solid build platform and thereby cannot withstand the forces of thermal shrinkage as the layers solidify. In further development of this method, it is suggested to include a multi-layer starting platform, where support structures can be added to minimize the warping issues. However, even the single-layer quasi-platform performed well in this experiment, as shown in Figure 2a. As can be seen in Figure 2a,b, the powder cake is divided into three layers, whose interfaces are indicated by arrows in the figures. The top layer is sintered by the EB during the PBF-EB process, the middle layer

is the NIR-sintered platform and the lower layer is a result of thermal sintering (TS) during the full process. The middle layer is the most sintered (the hardest) of the three layers, and the lower layer is the least sintered. As can be seen in Figure 2c, there is a distinct difference between the EB-sintered powder, which has visible lines from the EB rastering, while the NIR-sintered area has an even texture. Similar observations were also made for NIR versus EB heating in earlier publications [47]. Figure 2d shows that the quasi-platform is easily removed by PRS, which simplifies post-processing, as the parts can be built unattached to any build platform. This also shows the potential of varying the powder-cake hardness by NIR sintering without causing partial melting, which is often the case when too-intense EB sintering is applied [47].

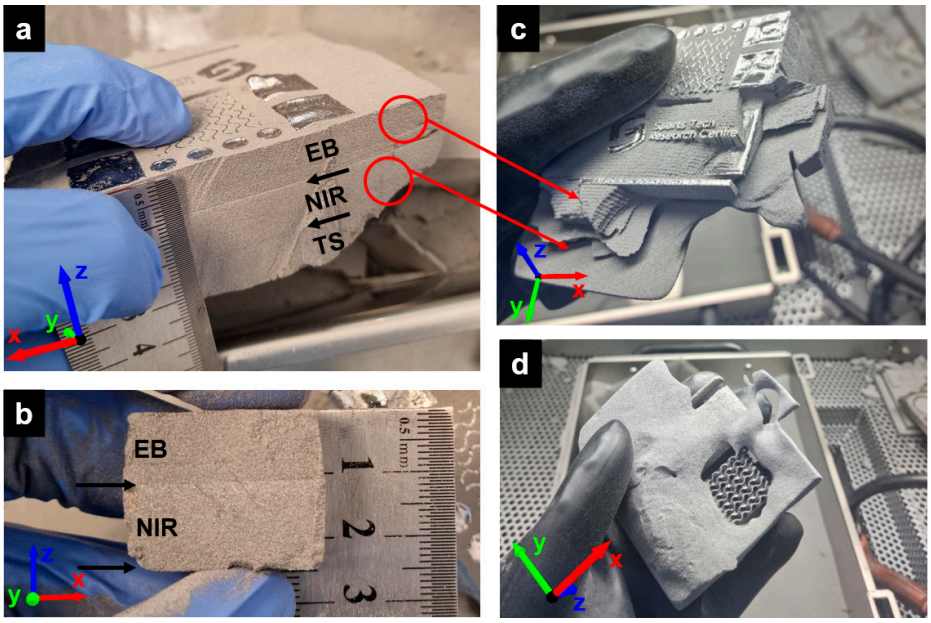

Figure 2. The parts built on a quasi-platform inside the resulting powder cake (**a**). A piece of the powder cake showing the structure of the NIR-sintered area, the EB-sintered area and the thermally sintered (TS) area below the quasi-platform (**b**). The powder removal process in the PRS system is shown from top (**c**) and bottom (**d**).

The samples manufactured on an NIR-sintered starting platform came out similar to those produced via the standard PBF-EB process, except for the previously mentioned warping of the first layers and a slight swelling on some of the parts (visible in Figures 2c and 2a, respectively). This indicates that the power input was slightly too high during the process, but it could also be an indication that the process temperature was too high for the selected printing parameters. Considering that the parameters were developed for a scenario where the thermal extraction is likely to be higher due to the difference in density between a build platform and a quasi-platform, this is a logical outcome.

In cross section, some very interesting features could be observed, indicating that it can be beneficial to avoid a build platform. The sample manufactured on a build platform showed significant contamination from contact with the build platform, as shown in Figure 3a,b. Elements from the build platform (304 stainless steel) were mixed and diffused into the Ti-6Al-4V, causing inhomogeneities in the microstructure (Figure 3c). Bruno et al. observed similar microstructures close to the build platform but did not mention or analyze any contamination [29]. The contamination was confirmed by EDX data (Figure 3d), where elements from the stainless steel could be found both in the grain boarders and as islands inside the grains in the lower parts of the samples. A significant number of pores could also be found in these regions, as can be seen in Figure 3b. The density of pores was highest in the region close to where the contamination stopped. It is not clear why the pores formed

here, but as nothing similar could be seen in the samples manufactured without the build plate, it is assumed to have arisen due to the incompatibility between the two alloys.

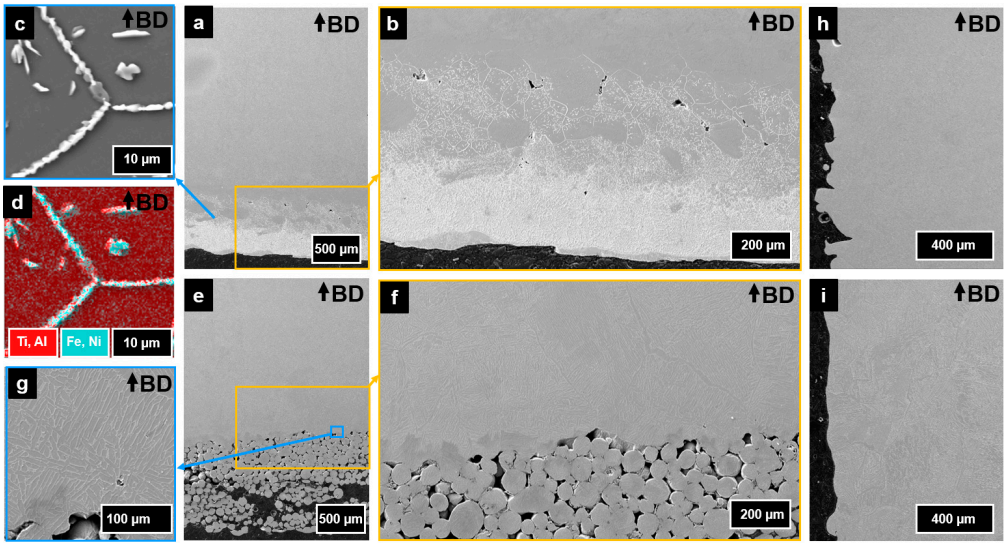

Figure 3. Cross section of the lower part (**a**,**b**) of one sample manufactured on top of a build platform, with a higher-magnification image of the microstructure (**c**) and EDX mapping results for the same region (**d**). Cross section of the lower part of one sample manufactured without a build platform (**e**,**f**), with a higher-magnification image of the microstructure, where the Widmanstätten structure is visible at the very bottom of the build (**g**). Cross sections showing the surface roughness of samples manufactured with a build platform (**h**) and without a build platform (**i**).

Samples manufactured on the quasi-platform did not show any clear inhomogeneities in their microstructures, and there was a significantly smaller number of pores, as shown in Figure 3e–g. The few pores that did exist were also on a smaller scale when compared to samples manufactured on a build platform (e.g., Figure 3g vs. Figure 3f). A large amount of semi-melted powder particles originating from the quasi-platform could be observed to be attached to the bottom of the sample (Figure 3e,f). Another interesting observation was that the vertical surfaces came out smoother in the build performed on a quasi-platform (Figure 3h vs. Figure 3i). This observation could be made in several locations on all examined samples. Unfortunately, the samples produced in this work were too small to perform profilometry, and the warping of the lower layers made further analyses of the surface roughness difficult, so it should be further studied when producing larger samples.

Figure 4a,b further show how the contamination was distributed throughout the lower part of the samples built on top of a build platform. As can be seen from the EDX map in Figure 4b, the contamination was quite evenly distributed in the lower region of the sample and gradiently decreased as the build progressed, where some islands of cleaner Ti-6Al-4V appeared before moving into "uncontaminated" material. Cracks were observed in the contaminated areas, one example of which is shown in Figure 4a. Nanoindentation (Figure 4c,d) confirmed that the mechanical properties were skewed close to the build platform and would decrease the performance of any part manufactured in this region. The low parts of Figure 4c,d show significantly harder and stiffer material where the contamination is present. It is likely that this increase in hardness in combination with defects between Ti-6Al-4V and the 304 stainless steel resulted in the cracks originating in the interface at the build plate. An interesting note is that no cracks could be observed in the quasi-platform case, even though there were plenty of possible initiation sites, as shown in Figure 3f. A less likely contribution to the cracks may be made by oxygen pickup close to the build plate [52].

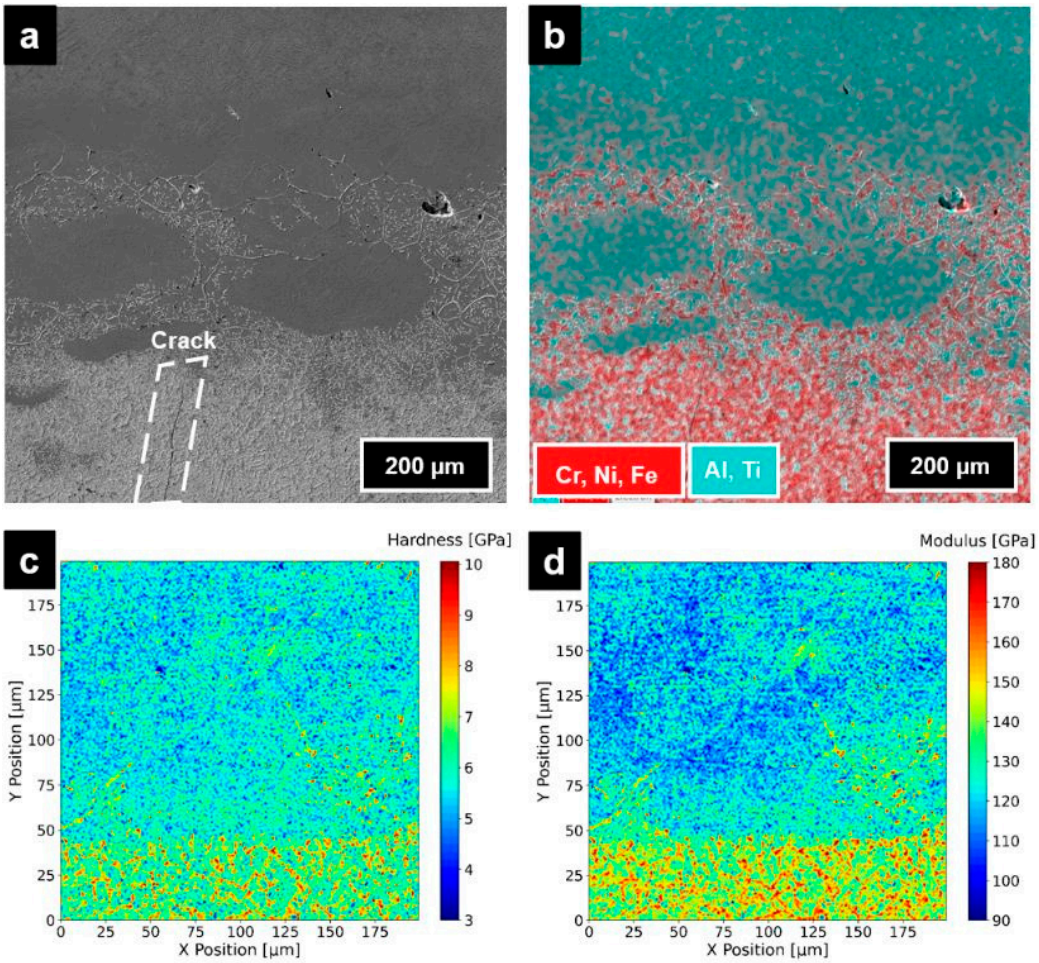

Figure 4. Cross section of the contamination in the samples built on a build platform (**a**) overlaid by EDX mapping (**b**). (**c**,**d**) Results from 200 × 200 nanoindentations in a similar region.

A smoother surface could also be noted on the overhanging surfaces of the TPMS lattices when comparing the samples manufactured on a quasi-platform (Figure 5a) to the ones manufactured on a stainless-steel build platform (Figure 5b). The close-up images in Figure 5c,d indicate that this difference seems to be mainly due to a smaller amount of powder particles add-sintered to the surfaces of the samples produced without build platforms. This is believed to be due to the more focused and short application of the EB in each point, resulting in large local thermal peaks (as opposed to the NIR heating, which is more evenly applied over the whole area). It can also be speculated that more heat is retained in the build volume when a build platform is not present.

Hardness measurements and further microscopical studies in Figure 6 show that the microstructural evolution throughout the builds is different. The hardness close to the build platform is significantly higher coupled to the heterogeneous microstructure (as shown earlier in Figure 4c). The hardness close to the quasi-platform is instead lower, and the typical PBF-EB [52,59] acicular α laths with β phase along the borders are already present. Higher up in the builds, the main difference between the samples manufactured with or without a build platform is the β-phase grain size and the α-lath size. It can be speculated that the presence of a build platform allows quicker heat transfer and thereby a smaller grain size, as the solidification time of each layer is faster. This directly indicates that the heat retention is better in the quasi-platform case, which correlates well with the differences in surface finish observed earlier. The resulting microstructure towards the top in Figure 6c,f is likely due to the difference in annealing time leading to fewer transformations and potentially the retention of some α′ phase, as explained by Davids et al. [53].

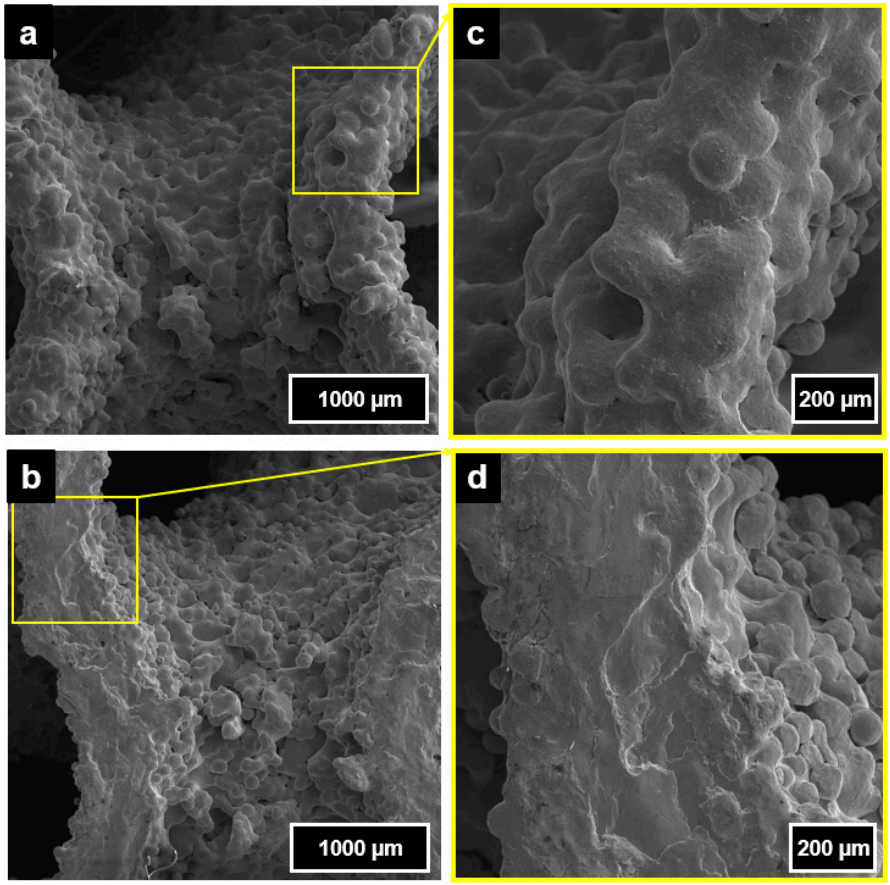

Figure 5. SEM view from the lower side of triply periodic minimal surface lattices manufactured without a build platform (**a**) and with a build platform (**b**), as well as close-ups of the bottom surfaces of these (**c**,**d**, respectively).

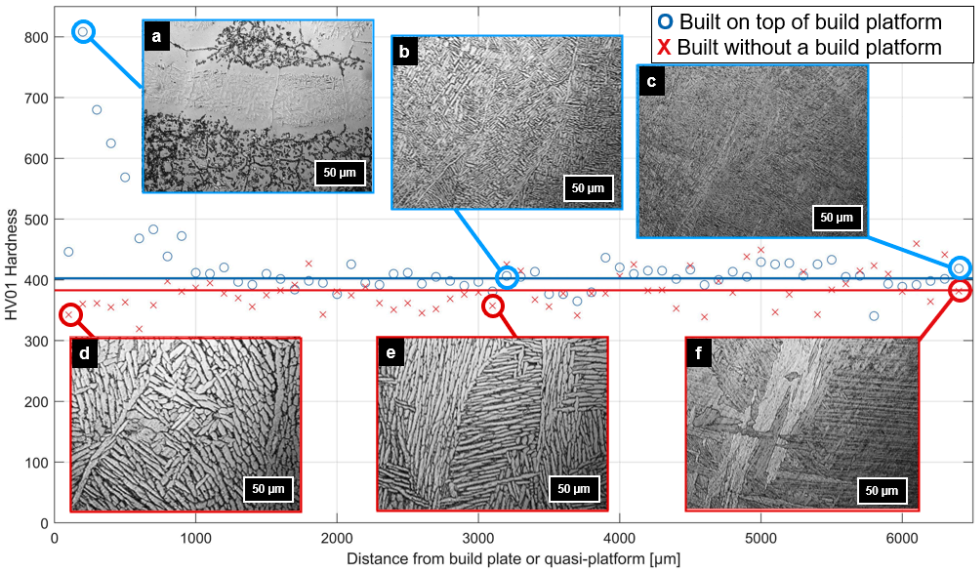

Figure 6. Vickers HV01 hardness plots of samples built on a build platform and on a quasi-platform overlaid by microstructural images of each sample at various heights (**a**,**b**,**c** and **d**,**e**,**f** respectively). The horizontal lines spanning the plot correspond to the average bulk hardness of the sample built on top of a build platform, 403 HV01 (standard deviation: 20), and the sample built without a build platform, 383 HV01 (standard deviation: 29). The bulk hardness was calculated from the average between 2000 and 6000 µm from the build platform.

3.2. Repairing by NIR-Assisted PBF-EB

The brief sintering of the loose powder bed (4 min) allowed a powder cake to form, as shown in Figure 7a. However, as shown by the emittance in Figure 7b, the main heat was confined to the spoon and melt area, which seemed to absorb more of the NIR energy. Figure 7c shows the teaspoon with the logo built on top, as it was removed from the build chamber. As can be seen in Figure 7d, the "repair" was successful in fusing the two materials on a microstructural level. The fine, equiaxed microstructure of the teaspoon was mostly preserved up to about ~100 µm from the interface, where columnar grains formed towards the 316L material. These columnar grains were likely the result of a slight remelting of the spoon surface and later annealing with a directional heat flow away from the heated area (top). The preservation of the original microstructure in the lower section indicates that an optimized process could be tuned to unite the two material structures, as PBF-EB is known for good microstructural control [43,60–62]. The EDX analysis of the transition in Figure 7e utilized the fact that 316L has a higher Ni content than 304 stainless steel. By overlaying the Fe signal with the Ni signal, the mixing of compositions throughout the transition can be estimated. This indicates that in some areas the transition was direct, and in some areas the two alloys were mixed together and created a gradient transition, as shown in Figure 7e.

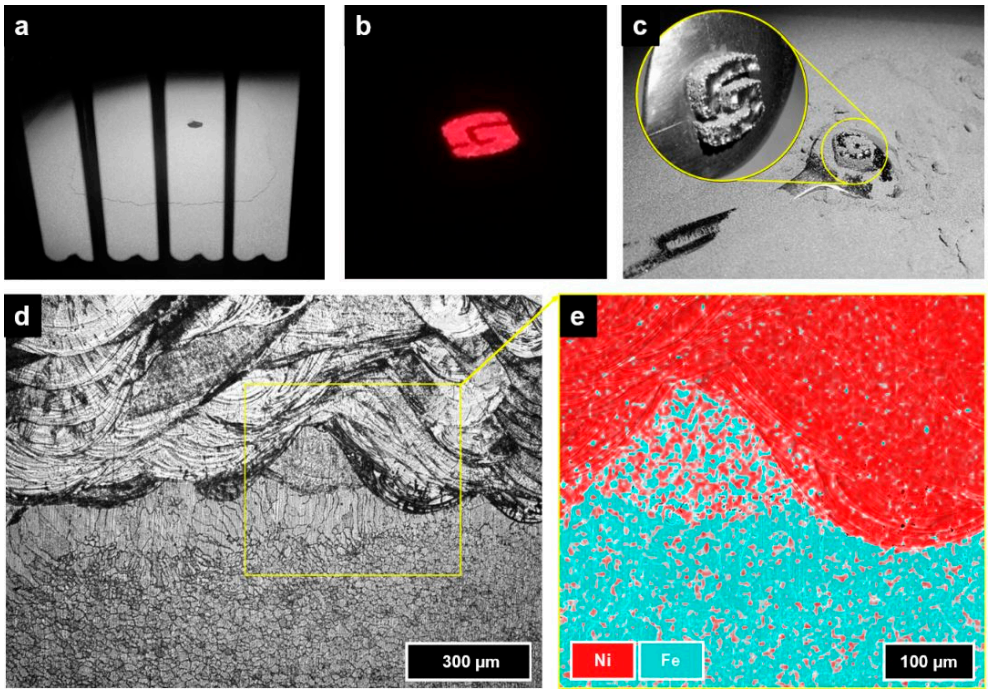

Figure 7. Spoon placed in powder bed after initial NIR heating (**a**). Logo melted on top of spoon, showing that only the spoon and melted parts were hot (**b**). Spoon with logo built on top after the process (**c**) and a cross section of the transition (**d**) as well as an energy-dispersive X-ray analysis of the transition (**e**).

4. Conclusions

The aim of this work was to investigate some of the benefits of using NIR in the PBF-EB process. This work shows that heating by NIR enables elimination of the build platform as well as repairs of parts placed in a loose powder bed in PBF-EB. The elimination of the build platform lowers the preparation time, waste and cost for one build, which represents a competitive enhancement. Removing the build platform was also shown to lower the risk of component or powder contamination, yielding an even cleaner process. The samples manufactured without a build platform showed similar hardness properties to standard PBF-EB samples. However, the surface was noted to be smoother and the microstructure

coarser and less heterogeneous in the initial millimeters, which could prove beneficial for components close to the bottom of a build. The improvement in surface finish is likely the effect of having a homogeneous constant heating input compared to the fast sweeping of the electron beam. The main drawback is the slight warpage of the lower layers; it is suggested that further developments of the NIR-sintered quasi-platform could solve this by integrating several heating steps in combination with EB support. It was also shown that NIR heating allows builds on top of parts placed in the loose powder bed. This simplifies repairing by PBF-EB as compared to the previous method of machining a build platform to fit the part in need of repairing. In the presented case, the build file was aligned simply by centering the beam in a predefined location. For complex repairs, more points of reference could be needed.

There are further optimizations still needed, such as adjusting the process themes, which in this case resulted in swelling due to excessive heat input. Furthermore, the heat model is not valid without the build platform, so adjustments in the control system, as well as additional temperature sensors, are needed before full automatization of the process. However, the presented results prove the feasibility of the suggested processes.

Author Contributions: Conceptualization and funding acquisition, L.-E.R. Methodology, setup, investigations and analysis, W.S. Microscopy, W.S. and C.B. Nanoindentation and related data analysis, L.O.M. and W.S. Writing—original draft preparation, all authors. Writing—review and editing, W.S. and L.O.M. Visualization, L.-E.R. Supervision and Application for funding, L.-E.R. All authors have read and agreed to the published version of the manuscript.

Funding: The work was partly financed by the Enströms Foundation through the Pro-A project.

Data Availability Statement: Contact the corresponding author for access to the data.

Acknowledgments: The authors would like to thank Kai K. O. Bär, Rolf Wirth (adphos Innovative Technologies GmbH) and Karl Neulinger (St. Pölten, AUT) for their contributions and for participation in the presented investigations. We would also like to gratefully acknowledge the adphos Group for the near-infrared equipment and test setup provision.

Conflicts of Interest: The authors declare no conflicts of interest.

References

1. Carolo, L.C.B.; Cooper, O.R.E. A review on the influence of process variables on the surface roughness of Ti-6Al-4V by electron beam powder bed fusion. *Addit. Manuf.* **2022**, *59*, 103103. [CrossRef]
2. Fu, Z.; Körner, C. Actual state-of-the-art of electron beam powder bed fusion. *Eur. J. Mater.* **2022**, *2*, 54–116. [CrossRef]
3. Botero, C.; Ramsperger, M.; Selte, A.; Åsvik, K.; Koptyug, A.; Skoglund, P.; Roos, S.; Rännar, L.-E.; Bäckström, M. Additive Manufacturing of a Cold-Work Tool Steel using Electron Beam Melting. *Steel Res. Int.* **2020**, *91*, 1900448. [CrossRef]
4. Sjöström, W.; Botero Vega, C.A. Feasibility of Electron Beam Melting Metal Coated Ceramic Powders. 2023. Available online: https://urn.kb.se/resolve?urn=urn:nbn:se:miun:diva-46817 (accessed on 28 April 2023).
5. Sjöström, W.; Botero, C.; Jimenez-Pique, E. Coating as a Methodology to Increase Processability of Al_2O_3 in Electron Beam Powder Bed Fusion. 2023. Available online: https://urn.kb.se/resolve?urn=urn:nbn:se:miun:diva-48006 (accessed on 28 April 2023).
6. Kotzem, D.; Teschke, M.; Juechter, V.; Körner, C.; Walther, F. Microstructure analysis and mechanical properties of electron beam powder bed fusion (PBF-EB)-manufactured γ-titanium aluminide (TiAl) at elevated temperatures. *Mater. Test.* **2022**, *64*, 636–646. [CrossRef]
7. Kirchner, A.; Klöden, B.; Franke-Jurisch, M.; Rauh-Hain, L.I.; Weißgärber, T. Manufacturing of tool steels by PBF-EB. *Metals* **2021**, *11*, 1640. [CrossRef]
8. Mukherjee, P.; Gabourel, A.; Firdosy, S.A.; Hofmann, D.C.; Moridi, A. Additive manufacturing of refractory metals and carbides for extreme environments: An overview. *Sci. Technol. Weld. Join.* **2024**, *29*, 99–115. [CrossRef]
9. Grasso, M.; Colosimo, B.M. A review of the current state-of-the-art on in situ monitoring in electron beam powder bed fusion. *Prog. Addit. Manuf.* **2024**, *9*, 1449–1466. [CrossRef]
10. Sjöström, W.; Botero, C.; Jimenez-Piqueo, E. Melting ceramic Al_2O_3 powder by electron beam powder bed fusion. *Prog. Addit. Manuf.* **2024**, *9*, 1523–1535. [CrossRef]
11. Wennersten, K.; Xu, J.; Armakavicius, N.; Wiberg, A.; Najafabadi, H.N.; Moverare, J. Feasibility of Melting NbC Using Electron Beam Powder Bed Fusion. *Adv. Eng. Mater.* **2024**, *26*, 2301388. [CrossRef]
12. Rizza, G.; Galati, M.; Iuliano, L. Evaluation of the effective thermal conductivity of the unmelted powder particles during the electron beam powder bed fusion (EB-PBF) process. *Procedia CIRP* **2023**, *118*, 765–770. [CrossRef]

13. Gui, Y.; Aoyagi, K.; Chiba, A. Development of macro-defect-free PBF-EB-processed Ti–6Al–4V alloys with superior plasticity using PREP-synthesized powder and machine learning-assisted process optimization. *Mater. Sci. Eng. A* **2023**, *864*, 144595. [CrossRef]
14. Sing, S.L.; An, J.; Yeong, W.Y.; Wiria, F.E. Laser and electron-beam powder-bed additive manufacturing of metallic implants: A review on processes, materials and designs. *J. Orthop. Res.* **2016**, *34*, 369–385. [CrossRef]
15. Zhang, L.-C.; Liu, Y.; Li, S.; Hao, Y. Additive Manufacturing of Titanium Alloys by Electron Beam Melting: A Review. *Adv. Eng. Mater.* **2018**, *20*, 1700842. [CrossRef]
16. Antonysamy, A.A.; Parimi, L.L.; Mani, M.K.; Schade, C.T.; Lunt, A.J. Powder characterisation and the impact on part performance in electron beam melted Ti6Al4V. *Mater. Des.* **2024**, *239*, 112788. [CrossRef]
17. Rizza, G.; Galati, M.; Antonioni, P.; Iuliano, L. Effect of the Sintering Conditions on the Neck Growth during the Powder Bed Fusion with Electron Beam (PBF-EB) Process. *J. Manuf. Mater. Process.* **2023**, *7*, 55. [CrossRef]
18. Körner, C. Additive manufacturing of metallic components by selective electron beam melting—A review. *Int. Mater. Rev.* **2016**, *61*, 361–377. [CrossRef]
19. Milberg, J.; Sigl, M. Electron beam sintering of metal powder. *Prod. Eng.* **2008**, *2*, 117–122. [CrossRef]
20. Chiba, A.; Daino, Y.; Aoyagi, K.; Yamanaka, K. Smoke Suppression in Electron Beam Melting of Inconel 718 Alloy Powder Based on Insulator–Metal Transition of Surface Oxide Film by Mechanical Stimulation. *Materials* **2021**, *14*, 4662. [CrossRef]
21. Cordero, Z.C.; Meyer, H.M.; Nandwana, P.; Dehoff, R.R. Powder bed charging during electron-beam additive manufacturing. *Acta Mater.* **2017**, *124*, 437–445. [CrossRef]
22. Reith, M.; Franke, M.; Körner, C. Impact of the acceleration voltage on the processing of γ-TiAl via electron beam powder bed fusion. *Prog. Addit. Manuf.* **2023**, *9*, 1425–1436. [CrossRef]
23. Lee, H.-J.; Ahn, D.-G. Investigation of elimination of powder spreading in manufacture of thin and wide preheating beads from Co–Cr alloy powders using a P-ebeam. *J. Mater. Res. Technol.* **2021**, *14*, 1873–1883. [CrossRef]
24. Murr, L.E.; Martinez, E.; Amato, K.N.; Gaytan, S.M.; Hernandez, J.; Ramirez, D.A.; Shindo, P.W.; Medina, F.; Wicker, R.B. Fabrication of Metal and Alloy Components by Additive Manufacturing: Examples of 3D Materials Science. *J. Mater. Res. Technol.* **2012**, *1*, 42–54. [CrossRef]
25. Mandil, G.; Le, V.T.; Paris, H.; Suard, M. Building new entities from existing titanium part by electron beam melting: Microstructures and mechanical properties. *Int. J. Adv. Manuf. Technol.* **2016**, *85*, 1835–1846. [CrossRef]
26. Karimi, P.; Sadeghi, E.; Ålgårdh, J.; Harlin, P.; Andersson, J. Effect of build location on microstructural characteristics and corrosion behavior of EB-PBF built Alloy 718. *Int. J. Adv. Manuf. Technol.* **2020**, *106*, 3597–3607. [CrossRef]
27. Rahimi, F.; Pourabdollah, P.; Mehr, F.F.; Cockcroft, S.; Maijer, D. A macroscale heat transfer analysis of the build chamber in a commercial electron beam powder bed fusion (EB-PBF) additive manufacturing system during component fabrication. *Addit. Manuf.* **2023**, *78*, 103831. [CrossRef]
28. Kotzem, D.; Höffgen, A.; Raveendran, R.; Stern, F.; Möhring, K.; Walther, F. Position-dependent mechanical characterization of the PBF-EB-manufactured Ti6Al4V alloy. *Prog. Addit. Manuf.* **2022**, *7*, 249–260. [CrossRef]
29. Bruno, J.; Rochman, A.; Cassar, G. Effect of Build Orientation of Electron Beam Melting on Microstructure and Mechanical Properties of Ti-6Al-4V. *J. Mater. Eng. Perform.* **2017**, *26*, 692–703. [CrossRef]
30. Derimow, N.; Romero, A.; Rubio, A.; Terrazas, C.; Medina, F.; Wicker, R.; Hrabe, N. Sintered powder oxidation variation as a function of build height for titanium alloy produced by electron beam powder-bed fusion. *Addit. Manuf. Lett.* **2021**, *1*, 100023. [CrossRef]
31. Ye, J.; Chen, T.; Körner, C. Correlating outgassing and smoke phenomenon in electron beam powder bed fusion of Ti6Al4V using a residual gas analyzer. *Prog. Addit. Manuf.* **2024**. [CrossRef]
32. Javidrad, H.R.; Javidrad, F. Review of state-of-the-art research on the design and manufacturing of support structures for powder-bed fusion additive manufacturing. *Prog. Addit. Manuf.* **2023**, *8*, 1517–1542. [CrossRef]
33. Gil, E.; Mancisidor, A.M.; Iturrioz, A.; Garciandia, F.; Sebastian, M.S. Cracking susceptibility of maraging parts manufactured by laser powder bed fusion additive manufacturing: Study on the powder characteristics and baseplate preheating influence. *Powder Met.* **2023**, *66*, 416–426. [CrossRef]
34. Borrelli, R.; Bellini, C.; Berto, F.; Di Cocco, V.; Foti, P.; Iacoviello, F.; Mocanu, L.P.; Pirozzi, C.; Razavi, N.; Franchitti, S. The impact of Ti6Al4V powder reuse on the quality of electron beam powder bed fusion parts. *Prog. Addit. Manuf.* **2024**, *9*, 1475–1490. [CrossRef]
35. Kumaran, M. Experimental Investigations on Directed Energy Deposition Based Repair of Stainless Steel 316L Alloy Substrate Manufactured through Hot Rolled Steel and Powder Bed Fusion Process. *J. Mater. Eng. Perform.* **2023**, *32*, 5837–5848. [CrossRef]
36. Wurst, J.; Ganter, N.V.; Ehlers, T.; Schneider, J.A.; Lachmayer, R. Assessment of the ecological impact of metal additive repair and refurbishment using powder bed fusion by laser beam based on a multiple case study. *J. Clean. Prod.* **2023**, *423*, 138630. [CrossRef]
37. Megahed, S.; Koch, R.; Schleifenbaum, J.H. Laser Powder Bed Fusion Tool Repair: Statistical Analysis of 1.2343/H11 Tool Steel Process Parameters and Microstructural Analysis of the Repair Interface. *J. Manuf. Mater. Process.* **2022**, *6*, 139. [CrossRef]
38. Leino, M.; Pekkarinen, J.; Soukka, R. The role of laser additive manufacturing methods of metals in repair, refurbishment and remanufacturing—Enabling circular economy. *Phys. Procedia* **2016**, *83*, 752–760. [CrossRef]
39. Sato, N.; Matsumoto, M.; Ogiso, H.; Sato, H. Challenges of Remanufacturing Using Powder Bed Fusion Based Additive Manufacturing. *Int. J. Autom. Technol.* **2022**, *16*, 773–782. [CrossRef]

40. Hinojos, A.; Mireles, J.; Reichardt, A.; Frigola, P.; Hosemann, P.; Murr, L.E.; Wicker, R.B. Joining of Inconel 718 and 316 Stainless Steel using electron beam melting additive manufacturing technology. *Mater. Des.* **2016**, *94*, 17–27. [CrossRef]
41. Wang, L.; Li, Y.; Zhou, L.; Lou, Y.; Liu, S.; Zheng, D.; Yi, M. Progress in additive manufacturing, additive repair and fatigue evaluation of aviation titanium alloy blades. *Mater. Res. Lett.* **2023**, *11*, 973–1012. [CrossRef]
42. Chen, Y.; Yin, Y.; Yi, M. Powder bed fusion repair of titanium with surface damage: Molecular dynamics study on microstructure and mechanical properties. *Addit. Manuf.* **2024**, *84*, 104096. [CrossRef]
43. Tao, S.; Gao, R.; Peng, H.; Guo, H.; Chen, B. High-reliability repair of single-crystal Ni-base superalloy by selective electron beam melting. *Mater. Des.* **2022**, *224*, 111421. [CrossRef]
44. Terrazas, C.A.; Gaytan, S.M.; Rodriguez, E.; Espalin, D.; Murr, L.E.; Medina, F.; Wicker, R.B. Multi-material metallic structure fabrication using electron beam melting. *Int. J. Adv. Manuf. Technol.* **2014**, *71*, 33–45. [CrossRef]
45. Tosi, R.; Muzangaza, E.; Tan, X.P.; Wimpenny, D.; Attallah, M.M. Hybrid Electron Beam Powder Bed Fusion Additive Manufacturing of Ti–6Al–4V: Processing, Microstructure, and Mechanical Properties. *Met. Mater. Trans. A* **2022**, *53*, 927–941. [CrossRef]
46. Rock, C.; Tarafder, P.; Ives, L.; Horn, T. Characterization of copper & stainless steel interface produced by electron beam powder bed fusion. *Mater. Des.* **2021**, *212*, 110278. [CrossRef]
47. Sjöström, W.; Koptyug, A.; Rännar, L.-E.; Botero, C. Near-infrared radiation: A promising heating method for powder bed fusion Near-infrared radiation: A promising heating method for powder bed fusion. *Mater. Manuf. Process.* **2024**, *39*, 320–328. [CrossRef]
48. Taghian, M.; Mani, H.; Mosallanejad, M.; Abdi, A.; Saboori, A.; Iuliano, L. Critical Condition for Initiation of Dynamic Recrystallisation in Electron Beam Powder Bed Fused Ti-6Al-4V Alloy. *J. Alloys Compd.* **2024**, *1005*, 176165. [CrossRef]
49. Li, S.; Li, S.; Liu, H.; Liu, L.; Pan, D.; Wang, S.; Hui, D.; Wang, W.; Gao, L.; Gao, J.; et al. Microstructure and mechanical properties of large Ti6Al4V components by electron beam powder bed fusion. *Mater. Sci. Eng. A* **2024**, *913*, 147023. [CrossRef]
50. Sandell, V.; Åkerfeldt, P.; Hansson, T.; Antti, M.-L. Fatigue fracture characterization of chemically post-processed electron beam powder bed fusion Ti–6Al–4V. *Int. J. Fatigue* **2023**, *172*, 107673. [CrossRef]
51. Braun, D.; Ganor, Y.I.; Samuha, S.; Guttmann, G.M.; Chonin, M.; Frage, N.; Hayun, S.; Tiferet, E. A Design of Experiment Approach for Development of Electron Beam Powder Bed Fusion Process Parameters and Improvement of Ti-6Al-4V As-Built Properties. *J. Manuf. Mater. Process.* **2022**, *6*, 90. [CrossRef]
52. Shao, M.; Vijayan, S.; Nandwana, P.; Jinschek, J.R. The effect of beam scan strategies on microstructural variations in Ti-6Al-4V fabricated by electron beam powder bed fusion. *Mater. Des.* **2020**, *196*, 109165. [CrossRef]
53. Davids, W.J.; Chen, H.; Nomoto, K.; Wang, H.; Babu, S.; Primig, S.; Liao, X.; Breen, A.; Ringer, S.P. Phase transformation pathways in Ti-6Al-4V manufactured via electron beam powder bed fusion. *Acta Mater.* **2021**, *215*, 117131. [CrossRef]
54. Hadadzadeh, A.; Asadi, E.; Shakil, S.I.; Amirkhiz, B.S.; Mohammadi, M.; Haghshenas, M. Indentation-derived mechanical properties of Ti-6Al-4V: Laser-powder bed fusion versus electron beam melting. *Mater. Lett.* **2021**, *301*, 130273. [CrossRef]
55. Rännar, L.-E.; Koptyug, A.; Olsén, J.; Saeidi, K.; Shen, Z. Hierarchical structures of stainless steel 316L manufactured by Electron Beam Melting. *Addit. Manuf.* **2017**, *17*, 106–112. [CrossRef]
56. Wang, C.; Tan, X.; Liu, E.; Tor, S.B. Process parameter optimization and mechanical properties for additively manufactured stainless steel 316L parts by selective electron beam melting. *Mater. Des.* **2018**, *147*, 157–166. [CrossRef]
57. Zhong, Y.; Rännar, L.-E.; Liu, L.; Koptyug, A.; Wikman, S.; Olsen, J.; Cui, D.; Shen, Z. Additive manufacturing of 316L stainless steel by electron beam melting for nuclear fusion applications. *J. Nucl. Mater.* **2017**, *486*, 234–245. [CrossRef]
58. *ISO 6507-1:2023*; Metallic Materials—Vickers Hardness Test. Part 1: Test Method. The International Organization for Standardization: Geneva, Switzerland, 2023.
59. Ladani, L. Local and Global Mechanical Behavior and Microstructure of Ti6Al4V Parts Built Using Electron Beam Melting Technology. *Metall. Mater. Trans. A Phys. Metall. Mater. Sci.* **2015**, *46*, 3835–3841. [CrossRef]
60. Chauvet, E.; Tassin, C.; Blandin, J.-J.; Dendievel, R.; Martin, G. Producing Ni-base superalloys single crystal by selective electron beam melting. *Scr. Mater.* **2018**, *152*, 15–19. [CrossRef]
61. Li, Y.; Liang, X.; Yu, Y.; Wang, D.; Lin, F. Chinese Journal of Mechanical Engineering: Additive Manufacturing Frontiers Review on Additive Manufacturing of Single-Crystal Nickel-based Superalloys. *Chin. J. Mech. Eng. Addit. Manuf. Front.* **2022**, *1*, 100019. [CrossRef]
62. Ladani, L.; Sadeghilaridjani, M. Review of powder bed fusion additive manufacturing for metals. *Metals* **2021**, *11*, 1391. [CrossRef]